Low temperature growth of amorphous VO_2 films on flexible polyimide substrates with a TiO_2 buffer layer

Dae Ho Jung, Hyeon Seob So, Jae Seong Ahn, Hosun Lee, Trang Thi Thu Nguyen, Seokhyun Yoon, So Yeun Kim, and Haeng-Yoon Jung

Citation: Journal of Vacuum Science & Technology A **36**, 03E102 (2018); doi: 10.1116/1.5019388
View online: https://doi.org/10.1116/1.5019388
View Table of Contents: http://avs.scitation.org/toc/jva/36/3
Published by the American Vacuum Society

Low temperature growth of amorphous VO_2 films on flexible polyimide substrates with a TiO_2 buffer layer

Dae Ho Jung, Hyeon Seob So, Jae Seong Ahn, and Hosun Lee[a)]
Department of Applied Physics, Kyung Hee University, Yong-In 17104, South Korea

Trang Thi Thu Nguyen and Seokhyun Yoon
Department of Physics, Ewha Womans University, Seoul 03760, South Korea

So Yeun Kim
Center for Correlated Electron Systems, Institute for Basic Science (IBS), Seoul 08826, South Korea and Department of Physics and Astronomy, Seoul National University, Seoul 08826, South Korea

Haeng-Yoon Jung
Laser Research Center, Korea Photonics Technology Institute, Gwangju 61007, South Korea

(Received 13 December 2017; accepted 12 February 2018; published 28 February 2018)

Amorphous VO_2 thin films were grown on anatase TiO_2-buffered polyimide (PI) films using radio-frequency magnetron sputtering deposition with a VO_2 target as low as at 175 °C. For comparison, the authors grew VO_2 films on TiO_2-buffered SiO_2/Si substrates. The structural and morphological properties of the VO_2 films were evaluated by x-ray diffraction, field emission scanning electron microscopy, transmission electron microscopy, and Raman spectroscopy. VO_2 films grown on TiO_2/SiO_2/Si were crystalline at 200 and 250 °C and were amorphous at 175 °C. VO_2 films grown on TiO_2/PI were amorphous. No peak corresponding to the monoclinic phase of VO_2 appeared in the Raman spectra of VO_2/TiO_2/PI films grown at 175 or 200 °C. The chemical compositions of VO_2 and the binding energy spectra of V and O atoms were probed by x-ray photoelectron spectroscopy. The authors discussed the multivalence states of V atoms and oxygen vacancies based on the x-ray photoemission spectroscopy of crystalline and amorphous VO_2 films. The authors obtained the hysteresis curves of the resistivity as a function of temperature for both VO_2/TiO_2/SiO_2/Si and VO_2/TiO_2/PI films. In addition, the authors measured the reflectivity of VO_2/TiO_2/PI films below and above the metal-insulator transition temperature using spectroscopic ellipsometry. The reflectivity changed substantially and was comparable to the literature values of well-crystallized VO_2 films, even though the ratio of the switching resistivity values was as low as sixty. This work demonstrates that VO_2 films grown on plastic films grown at temperatures as low as 175 °C can be applicable as flexible thermochromic films for use in energy-saving windows. *Published by the AVS.* https://doi.org/10.1116/1.5019388

I. INTRODUCTION

Vanadium dioxide (VO_2) has been intensively studied mostly due to its near-room-temperature phase transition as well as its high phase stability. VO_2 undergoes a first-order metal-insulator transition (MIT) at $T_c = 67$ °C from a high-temperature metallic phase to a low-temperature insulating phase, which is accompanied by a structural phase transition from a high-temperature tetragonal (rutile, R) structure to a low-temperature monoclinic (monoclinic, M) structure.[1] VO_2 films that are highly transparent in visible-ultraviolet radiation in addition to the blockage of infrared solar radiation can be used for "solar control" windows. A thermochromic smart window is designed such that the VO_2 films regulate solar infrared radiation using the MIT phenomenon.[2]

For flexible smart-window applications, VO_2 films can be grown on plastic substrates such as polyimide (PI). Since the physical properties of plastic substrates degrade due to heating, it is desirable to lower the growth temperature of VO_2 films as low as possible. For example, the glass transition temperature of PI films (Kapton HN, Dupont) is between 360 and 410 °C, and the physical properties of PI films degrade even below 360 °C. In the literature, the growth temperature of VO_2 films was reported to be as low as 200 °C under certain conditions. For example, Zhang *et al.* performed 200 °C magnetron sputtering deposition of VO_2 thin films on glass substrates, where a substrate bias voltage of −160 V was applied.[3] However, the growth of VO_2 films using plastic substrates has seldom been reported in the literature,[4,5] and it is difficult to grow high quality VO_2 thin films directly on plastic substrates.[6] Kim *et al.* reported the growth of VO_2 films on graphene/polyethylene terephthalate.[7] However, processing including the transport of graphene films is time-consuming and annealing at 500 °C is required. Oxide buffer layers such ZnO, SnO_2, or TiO_2 were reported to decrease the growth temperature of VO_2 films to below 400 °C.[8,9] A TiO_2 buffer layer can be used for growing a VO_2 film on a flexible plastic substrate. The rutile phase of the TiO_2 buffer layer is known to increase the crystallinity of VO_2 films, to reduce the MIT temperature T_c of VO_2 films due to strain, and to reduce a possible diffusion of atoms

a)Electronic mail: hlee@khu.ac.kr

from substrates into VO_2 films.[8,9] For example, Miyazaki *et al.* reported that VO_2 films grown on TiO_2-buffered SiO_2/Si substrates showed poly-crystallinity, whereas VO_2 films grown on SiO_2/Si substrates were amorphous, below the growth temperature of 600 °C.[10] However, VO_2 films grown on anatase TiO_2 substrates or buffer layers have not been reported. We note that the anatase phase of TiO_2 is stable at room temperature (RT) and transforms slowly into the rutile phase at 610 °C under ambient pressure.[11]

Koza *et al.* reported that amorphous VO_2 films, which were grown using an electrodeposition method, showed resistive switching behavior as a function of driving current.[12] Youn *et al.* reported that the multiphase of VO_2, V_2O_3, and V_2O_5 crystalline films was grown on amorphous SiO_2/Si structure substrates.[13]

VO_2 films can have a minor phase of V_2O_3 and V_2O_5, either due to structural disorder originating from amorphization or due to oxygen deficiency and excess because the Magnéli phase (V_nO_{2n-1})[14] and the Wadsley phase (V_nO_{2n+1})[15] are stable at RT. Long range order is broken and short range order remains in amorphous VO_2 films, and this amorphization causes minor V_2O_3 and V_2O_5 phases as well as a main VO_2 phase. Even in crystalline VO_2 films, vanadium atoms can have V^{5+} and V^{3+} valence states as well as V^{4+} valence states, depending on the oxygen excess and deficiency, local defects, and residual impurities. Using charge neutrality, V^{3+} and V^{5+} states should occur, due to oxygen vacancies (deficiency) and excess in VO_2 films, respectively. The multivalence of vanadium atoms may affect the physical properties. For example, Youn *et al.* reported that the multivalence of V atoms affects the resistance-temperature (R-T) hysteresis behavior; this is because the minor phase of other valences (V^{5+} and V^{3+}) decreases the contrast of resistance as we change the stoichiometry of VO_{2+x} as a function of the V/O ratio.[16]

In this work, we investigated low temperature growth of amorphous VO_2 films grown on PI substrates through a buffer layer of anatase TiO_2 using RF sputtering deposition. In comparison, we grew VO_2 films on TiO_2-buffered SiO_2/Si substrates, and those grown at 250 and 175 °C were crystalline and amorphous, respectively. We found that VO_2/TiO_2/PI films grown at temperatures as low as 175 °C had a sizable regulation of the reflectivity of near-infrared light below and above T_c. In addition, they showed hysteresis in the resistivity with a change in the order of sixty even though VO_2 films were amorphous according to the Raman, transmission electron microscopy (TEM), and x-ray diffraction (XRD) measurements. The multivalence states of vanadium atoms and oxygen vacancies were discussed using the x-ray photoelectron spectroscopy (XPS) spectra of amorphous and crystalline VO_2 films.

II. EXPERIMENT

VO_2 thin films with a thickness of 55 nm were grown on TiO_2-buffered SiO_2/Si substrates and TiO_2-buffered PI films by RF magnetron sputtering deposition using a VO_2 target (ProTech) at temperatures ranging between 175 and 250 °C. We used Si (100) substrates with SiO_2 films that were 300 nm-thick. We also used 75 μm-thick PI films (Model: KAPTON HN, Dupont) as substrates. A TiO_2 buffer layer with a thickness of 200 nm was deposited at RT on SiO_2/Si substrates and on PI substrates by ion-beam assisted electron beam evaporation.[17] TiO_2 pellets were used as a source, and both the O_2 reactive gas and the Ar working gas were used. The chamber pressure was set at 2.25×10^{-5} Torr, and Ar and O_2 gas flow rates were 50 and 10 sccm, respectively. During sputtering deposition of the VO_2 films, the distance between the substrate and the target was 15 cm. The chamber pressure was set at 6 mTorr with an Ar flow of 10 sccm, and growth temperatures were varied as 175, 200, and 250 °C. After sputtering deposition, all the VO_2 films were annealed at the same deposition temperature for 40 min under an oxygen flow ranging from 0.275 to 1 sccm at the same chamber pressure.

The resistivities of the VO_2 films were measured using the four-point probe method (Keithley: Model 4200) during heating and cooling. The structural and morphological properties of the VO_2 films were measured using XRD, TEM, and field emission scanning electron microscopy (FESEM). XRD measurements were performed using a standard x-ray diffractometer with Cu Kα radiation. The surface morphologies of the VO_2 films were investigated using FESEM (Model: Merlin, Carl Zeiss). Field emission TEM (Model: Tecnai G2 F30 S, FEI) was used to probe the microstructure of the VO_2 films. The accelerating voltage of 300 kV was used for the TEM measurement. Raman scattering spectra were obtained using a McPherson 207 spectrometer equipped with a nitrogen-cooled charge-coupled-device array detector and a THMS600 Linkam cell temperature controller. The VO_2 films were excited using a 488 nm diode laser with a power of less than 0.5 mW to minimize heating effects. The reflectivity of the VO_2 films was measured at RT and 100 °C using ellipsometry (Model: V-Vase, J.A. Woollam Co.). XPS (Model: K-alpha, Thermoelectron) was used to determine the chemical shift of the binding energies of the VO_2 thin films and the depth profiles. Ar ions were used to etch the VO_2 thin films. The XPS spectra were calibrated with the O_{1s} peak.

III. RESULTS AND DISCUSSION

Figure 1 shows FESEM images of the surface of VO_2 films grown on (a) TiO_2/SiO_2/Si at 200 °C and (b) on TiO_2/PI substrates at 250 °C. The surface morphologies were generally flat except for the VO_2 films grown on TiO_2/SiO_2/Si substrates at 200 °C (weak grain boundary, average grain size of 10 nm) and grown on TiO_2/PI substrates at 250 °C (strong grain boundary, average grain size of 15 nm). The granular structures in the VO_2 films became weaker with the decreasing growth temperature, suggesting that the VO_2 films became more amorphous as the growth temperature decreased. This phenomenon was confirmed by XRD (Fig. 2) and Raman spectroscopy (Fig. 4).

Figure 2 shows the XRD patterns of the VO_2 films grown on the TiO_2/SiO_2/Si substrates at (a) 250 °C and (b)

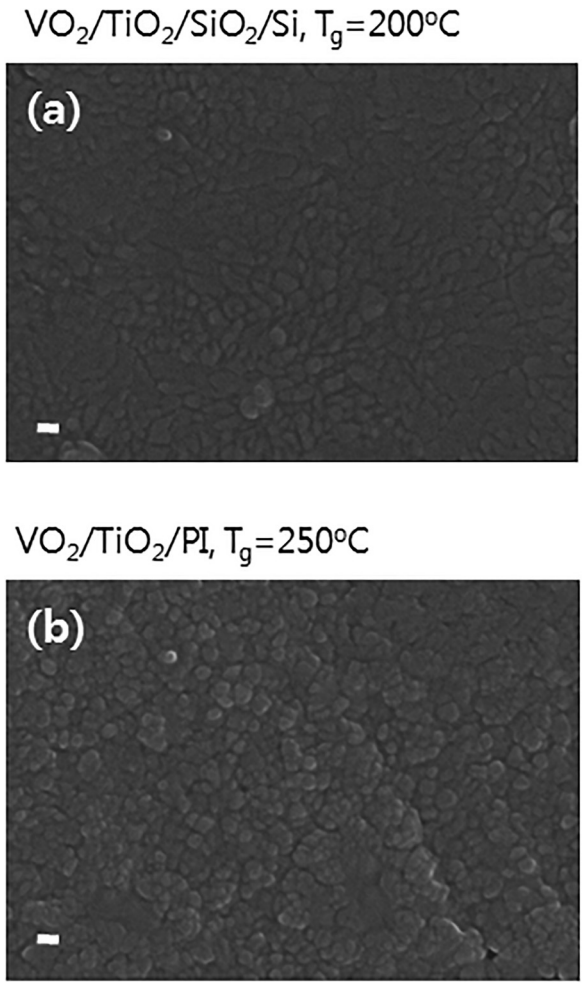

FIG. 1. FESEM images of the surface of VO_2 films grown on (a) $TiO_2/SiO_2/Si$ at 200 °C and on (b) TiO_2/PI at 250 °C. The scale bar represents 30 nm.

175 °C and grown (c) on TiO_2/PI at 175 °C. In Fig. 2(a), VO_2 films grown on $TiO_2/SiO_2/Si$ substrates at 250 °C showed crystalline peaks of VO_2 films at 27.97° (011), 55.24° ($\bar{2}13$), 55.58° (220)/(211), 57.75° (022), and 70.47° ($\bar{2}31$)/(202) and of TiO_2 films of the anatase phase at 25.39° (101), 48.19° (200), and 54.04° (105). The VO_2 peak at 55.24° could be overlapped with anatase TiO_2 (211), and the VO_2 peak at 70.47° could be overlapped with anatase TiO_2 (220).[18,19] In Fig. 2(b), the VO_2 films grown on $TiO_2/SiO_2/Si$ at 175 °C showed only a TiO_2 peak at 25.39° (101), resulting from the anatase phase. In Fig. 2(b), the peak at 33° originated from the Si substrate. In Fig. 2(c), no diffraction peaks of VO_2 and TiO_2 were observed in the XRD pattern for the VO_2 films grown on TiO_2/PI substrates at 175 °C, indicating that the VO_2 films as well as the TiO_2 buffer layer were amorphous.

Figure 3 shows (a) TEM image and (b) its fast Fourier transform (FFT) image of VO_2 films grown on TiO_2/PI at 250 °C. TEM data in Fig. 3 showed that the VO_2 films grown on TiO_2/PI substrates at 250 °C were amorphous.

Figure 4 shows the Raman spectra of the VO_2 films grown on $TiO_2/SiO_2/Si$ at (a) 200 °C and (b) 175 °C and on TiO_2/PI substrates at (c) 200 °C and (d) 175 °C as a function of the measurement temperature. For the $VO_2/TiO_2/SiO_2/Si$

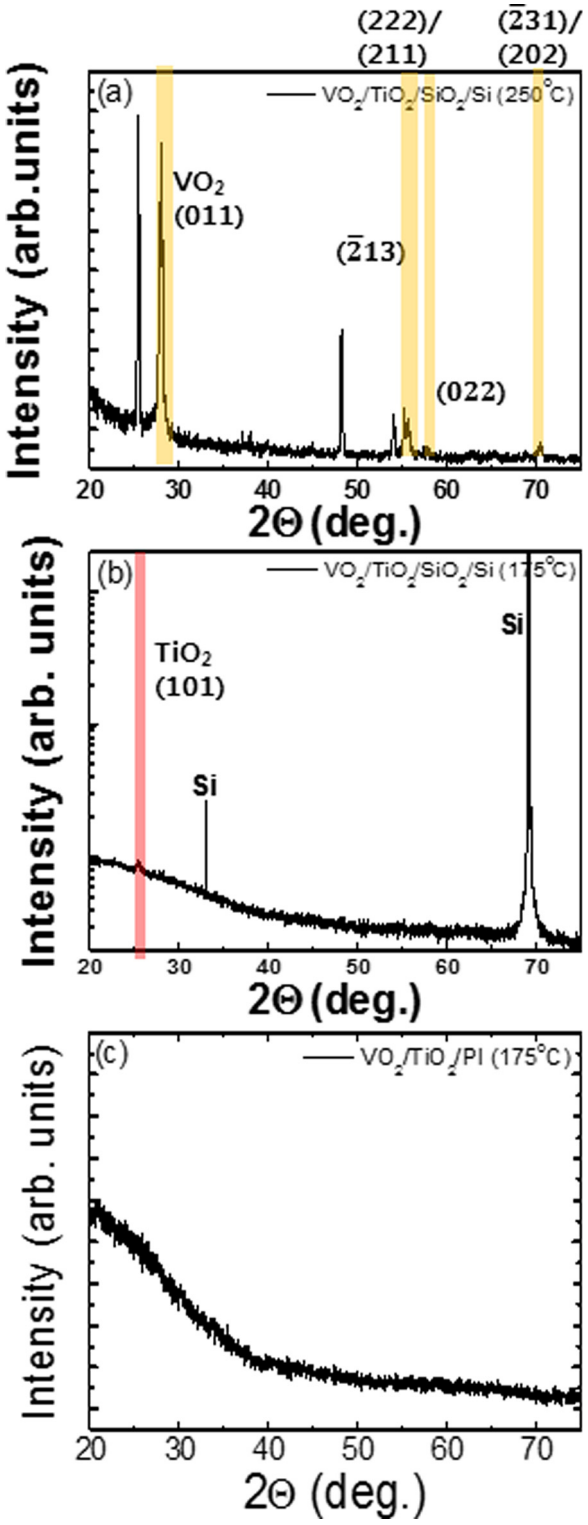

FIG. 2. (Color online) XRD patterns of the VO_2 films grown on $TiO_2/SiO_2/Si$ (a) at 250 °C and (b) at 175 °C and grown (c) on TiO_2/PI at 175 °C.

films grown at 200 °C, the 198 cm^{-1} peak is an A_g mode from the VO_2 films and 145.7, 393.4, and 635.2 cm^{-1} peaks correspond to the anatase TiO_2 buffer layer. The 520.4 cm^{-1} peak originated from the Si substrate and the 635.2 cm^{-1} peak could be explained as an overlap of the modes of both the VO_2 and TiO_2 films.

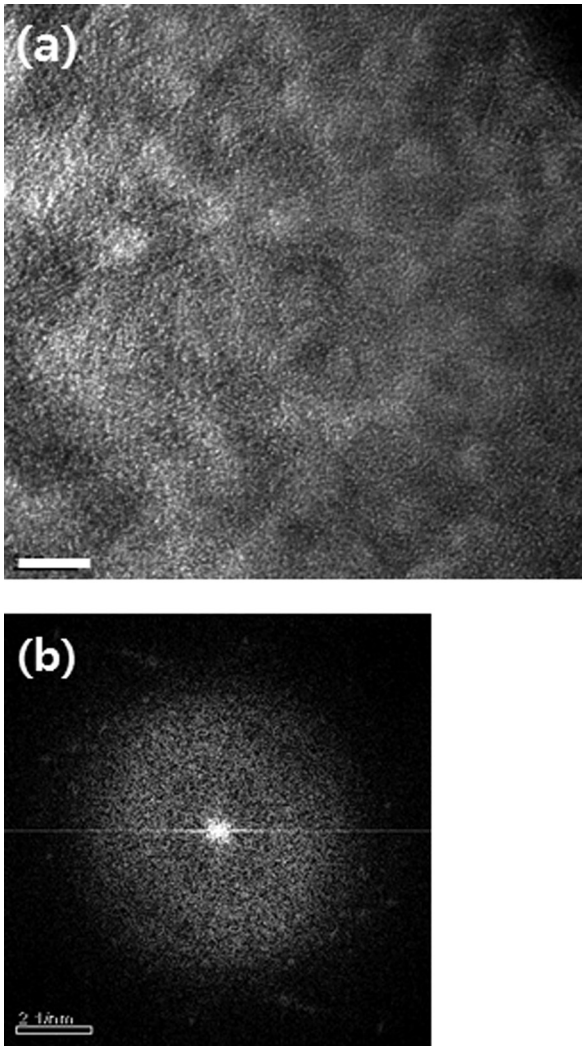

FIG. 3. (a) TEM image and (b) its FFT image of VO_2 films grown on TiO_2/PI at 250 °C. The scale bar represents 5 nm in (a).

We note that Raman spectra showed weak optical phonon peaks at 198.9 and 620.5 cm^{-1} for the VO_2 films grown on $TiO_2/SiO_2/Si$ at 250 °C (not shown here). In Figs. 4(c) and 4(d), VO_2 Raman peaks were not observed for VO_2/TiO_2/PI grown at 200 °C and 175 °C because the VO_2 films were amorphous. For the $VO_2/TiO_2/SiO_2/Si$ films, the monoclinic phase peak of VO_2 at 198 cm^{-1}, corresponding to V-V vibrations, was observed at RT in Fig. 4(a).[20] However, as the temperature was increased from RT to 100 °C, no phonon mode from the VO_2 rutile phase was observed. We observed only TiO_2-related peaks at 157.8 and 424.8 cm^{-1} from $VO_2/TiO_2/SiO_2/Si$ grown at 175 °C [Fig. 3(b)]. For VO_2/TiO_2/PI films grown at 200 and 175 °C, the 159 and 419 cm^{-1} peaks were a result of the TiO_2 anatase phase [Figs. 3(c) and 3(d)] and were blue-shifted from the bulk values 144 and 399 cm^{-1}, respectively, reported in the literature.[21] This result indicates that only amorphous films of VO_2 were formed at 200 and 175 °C for VO_2/TiO_2/PI films, which confirms the XRD of Fig. 2(c) and TEM data in Fig. 3. We note that the crystallinity of the TiO_2-buffer layer became poorer as the growth temperature decreased and that the crystallinity of the TiO_2-buffer layer was inferior for TiO_2/PI than $TiO_2/SiO_2/Si$ in terms of XRD (Fig. 2) and Raman spectra (Fig. 4). TiO_2-buffer layers consisted of the anatase phase for $VO_2/TiO_2/SiO_2/Si$ and were amorphous and anataselike for VO_2/TiO_2/PI. In Table I, we summarized the crystallinities of VO_2 films grown on $TiO_2/SiO_2/Si$ and TiO_2/PI at varying growth temperatures (T_g), which were determined using XRD, TEM, and Raman spectroscopy.

Figure 5 displays the XPS spectra of the binding energy for (a) O_{1s} and the oxygen vacancy (V_O) and (b) the multivalence state of $V_{2p3/2}$ for $VO_2/TiO_2/SiO_2/Si$ grown at 250 °C, as well as the same [(c) and (d)] for VO_2/TiO_2/PI grown at 175 °C.[22] The XPS binding energy spectra were calibrated using the O_{1s} peak energy at 530.0 eV, and the XPS spectra were taken just below the surface layers to remove natural oxides. We found the oxygen vacancy peak at 531.2 and 531.4 eV for crystalline [Fig. 5(a)] and amorphous [Fig. 5(c)] VO_2 films, respectively, and $I(V_O)/I(O_{1s})$ increased from 22.2% to 32.8% with increasing disorder. We found V^{5+} (517.1 eV), V^{4+} (515.7 eV), and V^{3+} (514.5 eV) peaks for the crystalline VO_2 films and V^{5+} (517.3 eV), V^{4+} (516.0 eV), and V^{3+} (515.2 eV) peaks for the amorphous VO_2 films. The V and O vacancies generate the V^{5+} and V^{3+} states, respectively.[14] VO_2 (in the V^{4+} state) films can have a minor phase of V_2O_3 (in the V^{3+} state) and V_2O_5 (in the V^{5+} state), which can occur because of structural disorder due to amorphization or oxygen deficiency/excess because the Magnéli phase (V_nO_{2n-1}) and the Wadsley phase (V_nO_{2n+1}) are stable at RT.[14,15]

The depth profile of the V and O atom compositions revealed the formation of stoichiometric VO_2 films for both VO_2 films in Fig. 5 (not shown here). The V composition increased slightly from 28.1 (28.0%) at the surface to 32.1% (29.4%) in the bulk, whereas the O composition decreased slightly from 71.9% (72.0%) to 67.9% (70.6%) in bulk for the crystalline $VO_2/TiO_2/SiO_2/Si$ ($T_g = 250$ °C) [amorphous VO_2/TiO_2/PI ($T_g = 175$ °C)] films. Considering the expected natural oxidation of VO_2 films at the surface, this result confirms the stoichiometric depth profile of the VO_2 films.

Figure 6 displays the thermal hysteresis of the resistivity of the VO_2 thin films grown on $TiO_2/SiO_2/Si$ at (a) 250 °C, (b) 200 °C, and (c) 175 °C as well as those grown on TiO_2/PI at (d) 250 °C, (e) 200 °C, and (f) 175 °C during heating and cooling. All the VO_2 films showed MIT behavior. In Figs. 6(a)–6(c), as the growth temperature was decreased, the resistivities of the $VO_2/TiO_2/SiO_2/Si$ films changed at T_c from 1.670 Ω cm (insulating) to 0.56×10^{-3} Ω cm (metallic), 1.447 to 0.126×10^{-2} Ω cm, and 0.568 to 0.307×10^{-2} Ω cm at 250, 200, 175 °C, respectively. In Figs. 6(d)–6(f), with a decrease in the growth temperature, the resistivity of the VO_2/TiO_2/PI films changed at T_c from 0.164 to 0.279×10^{-2} Ω cm, 0.282 to 0.270×10^{-2} Ω cm, and 0.127 to 0.206×10^{-2} Ω cm, at 250, 200, and 175 °C, respectively. For the $VO_2/TiO_2/SiO_2/Si$ films, as the growth temperature increased, the sharpness of the MIT increased due to crystallization and the increased grain size. It has been reported that the sharpness of the resistivity hysteresis during MIT in polycrystalline VO_2 films increases with the increasing grain

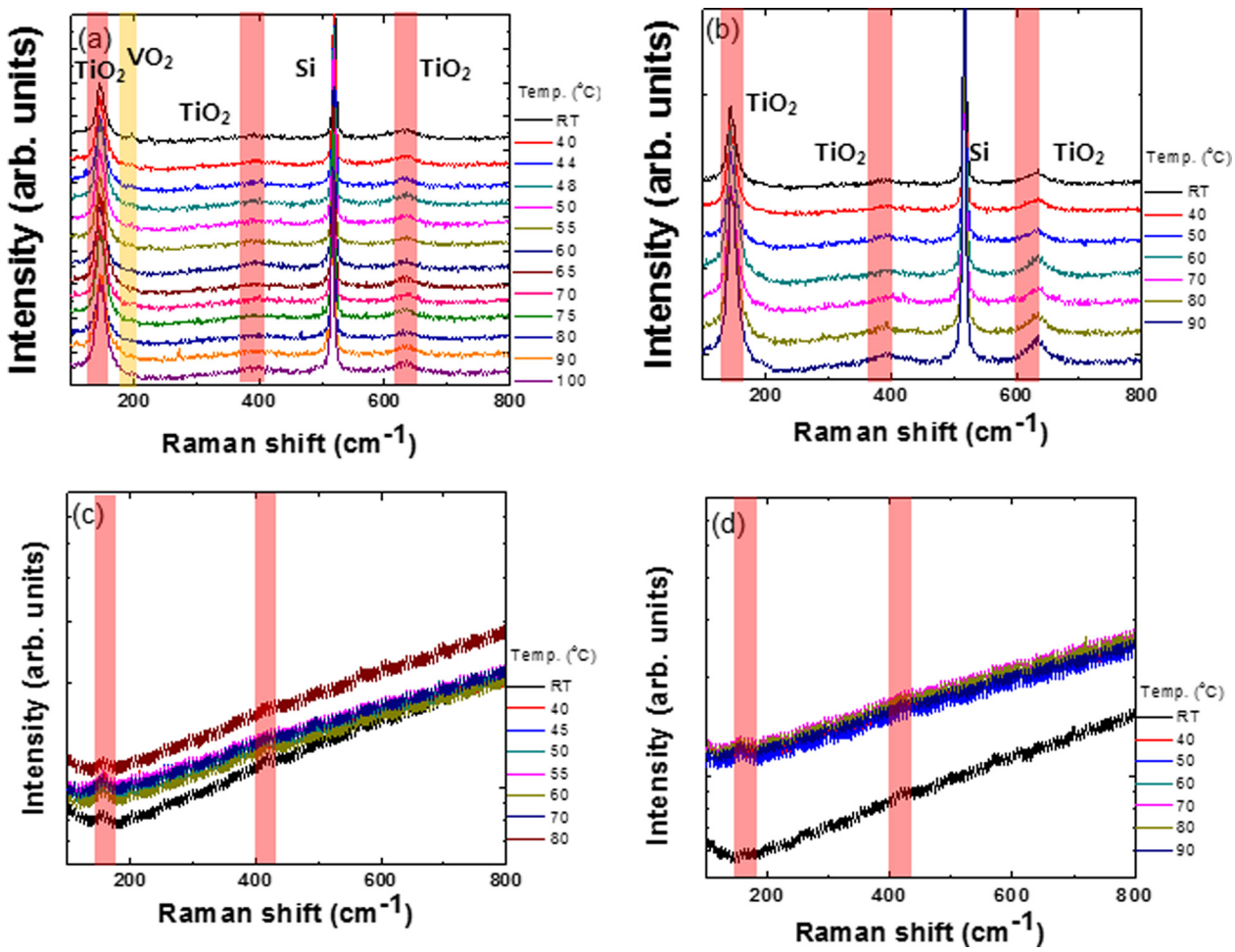

FIG. 4. (Color online) Raman spectra of the VO_2 films grown on $TiO_2/SiO_2/Si$ at (a) 200 °C and (b) 175 °C and on TiO_2/PI substrates at (c) 200 °C and (d) 175 °C, as a function of measurement temperature [red (thick) line: TiO_2; yellow (thin) line: VO_2].

size.[23] Similar explanations may apply to VO_2/TiO_2/PI films even though all the VO_2 films were amorphous. Other possible explanation is as follows: Long range crystalline order is missing in the amorphous VO_2 films. However, short range order may have increased in the amorphous VO_2 films with the increasing growth temperature, which may have increased the resistivity transition ratio.

We defined the ratio (ρ_r) of the transition of resistivity throughout the MIT as $\rho_r = \rho(20\,°C)/\rho(80\,°C)$. Figure 6 shows (a) the ratio (ρ_r) of resistivity during transition throughout the MIT as well as (b) the MIT transition temperature (T_c) and hysteresis width (ΔH) of the VO_2 films grown on $TiO_2/SiO_2/Si$ and TiO_2/PI substrates as a function of growth temperature. In Fig. 6(a), the ratio (ρ_r) of the resistivities of $VO_2/TiO_2/SiO_2/Si$ throughout the MIT was about 3 orders of magnitude and the ratio (ρ_r) of the transition of VO_2/TiO_2/PI was about 2 orders of magnitude at the growth temperature of 250 °C. The resistivity ratio (ρ_r) of VO_2/TiO_2/PI was still 2 orders of magnitude at the growth temperature of 175 °C. In Fig. 6, the relative changes of the resistivities (ρ_r) were 2.99×10^3, 1.15×10^3, and 1.85×10^2, and the MIT temperatures (T_c) were 42.6, 49.5, and 42.1 °C for the $VO_2/TiO_2/SiO_2/Si$ films with growth temperatures of 250, 200, and 175 °C, respectively. Likewise, the relative changes of the resistivities (ρ_r) were 58.8, 104.4, and 61.7, and the transition temperatures (T_c) were 36.0, 47.9, and 46.7 °C, respectively, for VO_2/TiO_2/PI films with growth temperatures of 250, 200, and 175 °C, respectively. The relative changes of the resistivities (ρ_r) were higher for crystalline $VO_2/TiO_2/SiO_2/Si$ films than for amorphous VO_2/TiO_2/PI films.

In Fig. 7(a), it is found that the relative changes of the resistivities (ρ_r) increased with increasing crystallinity because the VO_2 films grown on $TiO_2/SiO_2/Si$ substrates showed the Raman peaks for the VO_2 phase, while those

TABLE I. Crystallinities of VO_2 films grown on $TiO_2/SiO_2/Si$ and TiO_2/PI at varying growth temperatures (T_g), which were determined using XRD, TEM, and Raman spectroscopy.

	T_g (°C)	Crystallinity of VO_2	Crystallinity of the TiO_2 buffer layer
VO_2/TiO_2/PI	250	Amorphous	Amorphous
	200		
	175		
$VO_2/TiO_2/SiO_2/Si$	250	Crystalline	Crystalline
	200	Crystalline	Crystalline
	175	Amorphous	Weakly crystalline

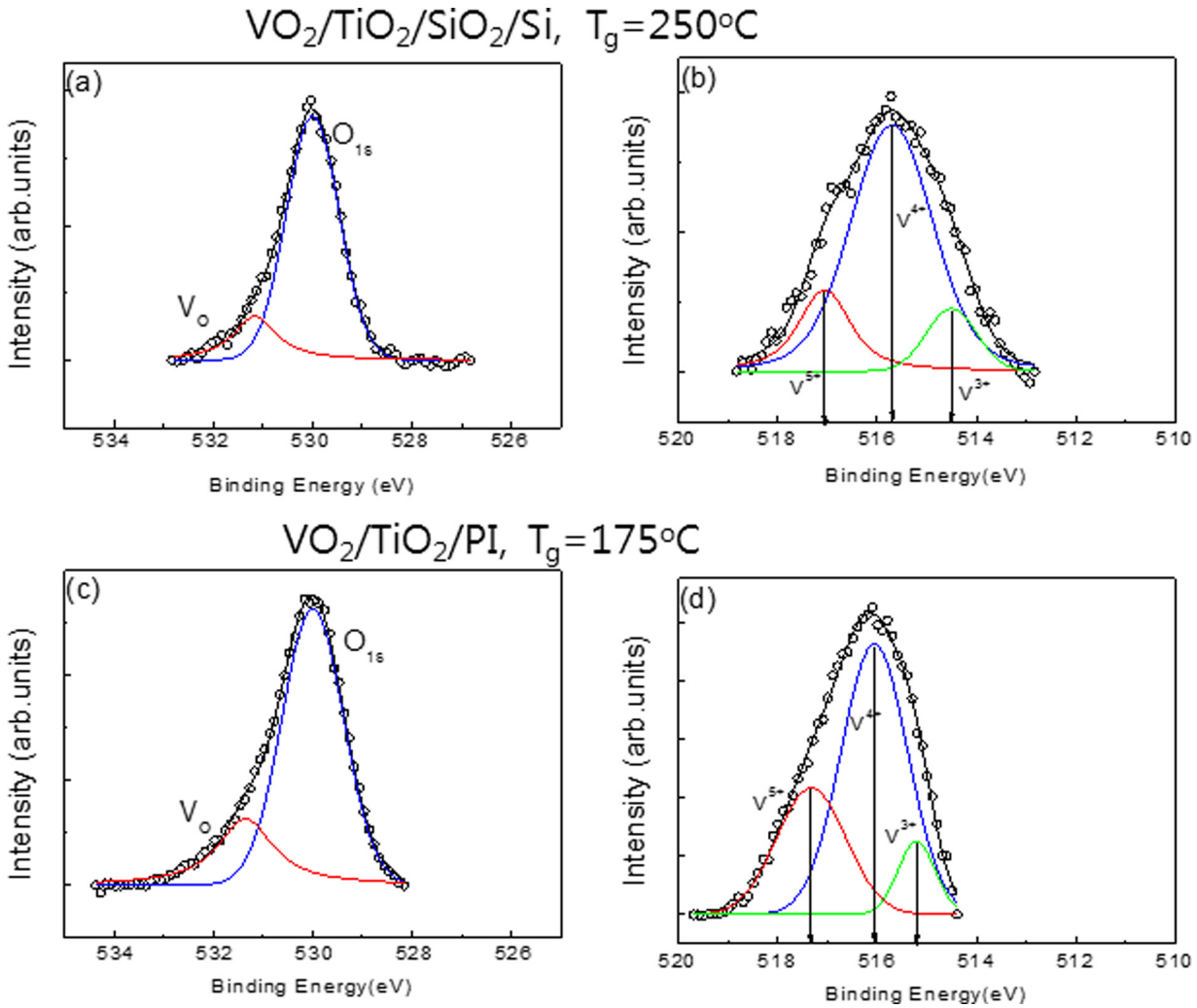

FIG. 5. (Color online) XPS spectra of the binding energy for (a) oxygen level (O_{1s}) and oxygen vacancy (V_O) and (b) multivalence state of $V_{2p3/2}$ for $VO_2/TiO_2/SiO_2/Si$ grown at 250 °C and the same [(c) and (d)] for $VO_2/TiO_2/PI$ grown at 175 °C.

grown on TiO_2/PI substrates did not show any. Furthermore, the relative changes of the resistivities (ρ_r) increased with increasing crystallinity because they increased with increasing growth temperature. The transition temperatures T_c (46.7 °C for T_g = 175 °C) for the VO_2 thin films grown on TiO_2-buffered PI were higher than those (42.1 °C for T_g = 175 °C) for VO_2 thin films grown on TiO_2-buffered SiO_2/Si. We potentially attribute the low T_c of the VO_2 thin films grown both on TiO_2-buffered PI and on TiO_2-buffered SiO_2/Si substrates to the small grain sizes in the VO_2 films. The transition temperature of both VO_2 films was lower than the bulk VO_2 value of 67 °C. The decrease in T_c can be caused by either the compression of the c_R (a_M) axis[24] or the small grain size.[25] For the $VO_2/TiO_2/SiO_2/Si$ films, the (011) VO_2 phase was the dominant phase and the a_M (i.e., c_R) axis was in-plane. Using the XRD patterns in Fig. 2(a), the lattice parameter was d (011) = 0.3186 nm. This value is smaller than the VO_2 bulk single crystal value of d (011) = 0.3203 nm. Therefore, the out-of-plane direction was under a compressive strain of -5.4×10^{-3}, and the in-plane direction was under a tensile strain of 2.9×10^{-3}. Because the c_R axis was in-plane and under tensile strain, the lowering of T_c cannot be explained in terms of the strain. VO_2 films grown on TiO_2/PI films were under tensile in-plane stress and compressive out-of-plane stress because $VO_2/TiO_2/PI$ films were rolled convex upward. Because the VO_2 films grown on TiO_2/PI were amorphous, there were no definite c_R axes. However, T_c was still reduced in VO_2/TiO_2/PI films compared to the bulk crystal values. T_c of a VO_2 film has also been reported to depend on the grain size of the VO_2 film. For example, Radue *et al.* found that T_c increased (decreased) with increasing (decreasing) average grain sizes.[25] In Fig. 1, the grain sizes were about 10 and 15 nm for $VO_2/TiO_2/SiO_2/Si$ grown at 200 °C and $VO_2/TiO_2/PI$ grown at 250 °C, respectively. However, the granular structures in other VO_2 films were not clear in the FESEM data, and the same explanation for low T_c cannot be applied. The low T_c values of the VO_2 films are possibly due to percolation of the oxygen-deficient region in VO_2 films.[26] As shown in Figs. 5(b) and 5(d), the VO_2 films in this work were inhomogeneous and consisted of oxygen-deficient (V^{3+}) and excess (V^{5+}) as well as stoichiometric VO_2 (V^{4+}) phases. According to Singh *et al.*, oxygen-deficiency in VO_2 films can cause reduction in T_c because oxygen vacancies in the

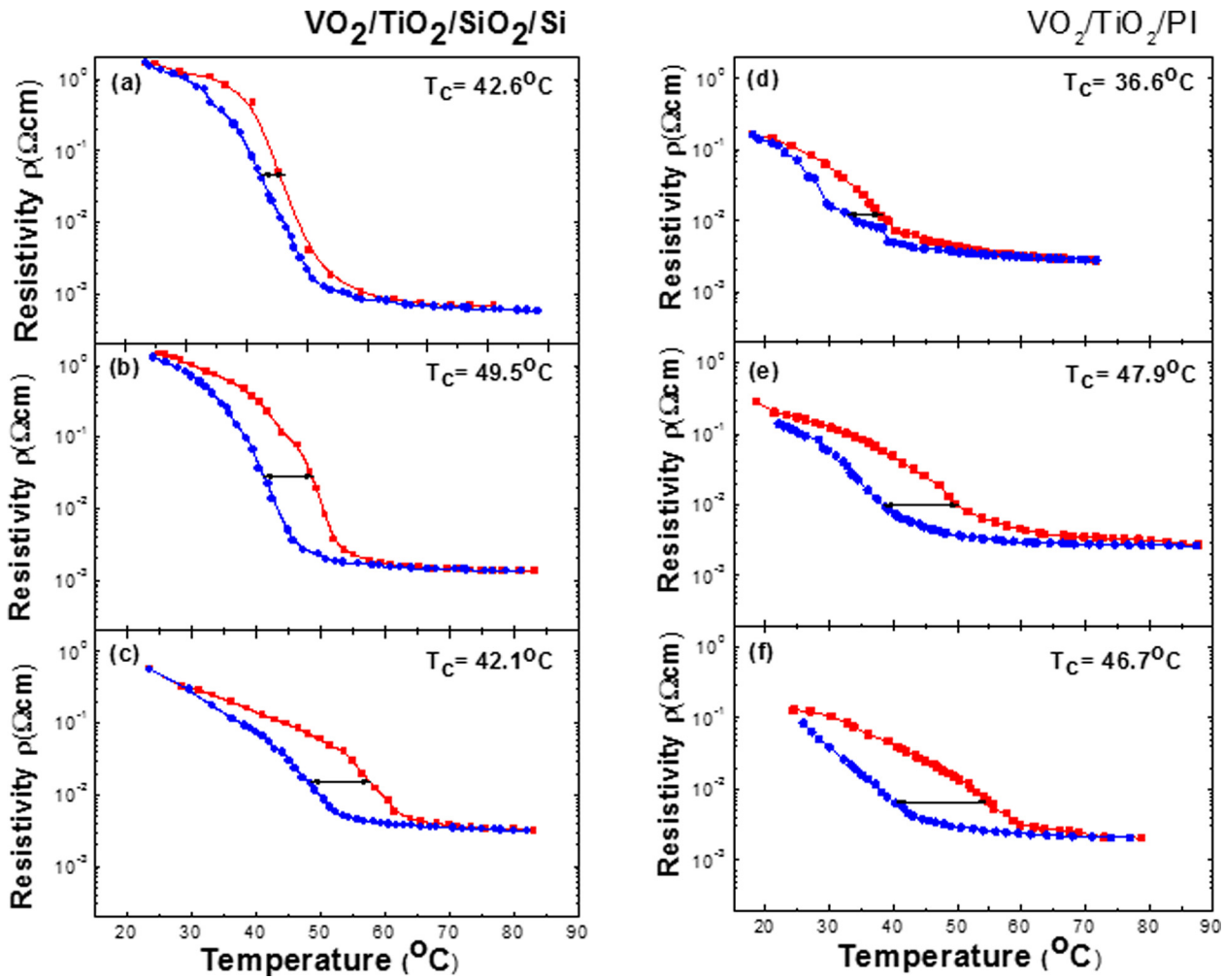

FIG. 6. (Color online) Thermal hysteresis of the resistivities of the VO_2 thin films grown on $TiO_2/SiO_2/Si$ at (a) 250 °C, (b) 200 °C, and (c) 175 °C and those grown on TiO_2/PI at (d) 250 °C, (e) 200 °C, and (f) 175 °C during heating (red squares) and cooling (blue circles). The arrow designates the hysteresis width (ΔH).

rutile VO_2 phase stabilize it by disrupting adjacent V-V chain dimerization required for a transition to the insulating monoclinic phase.[27]

In Fig. 7(b), the hysteresis width (ΔH) increased linearly with decreasing growth temperature and ΔH was larger for VO_2 films grown on TiO_2/PI than for those grown on $TiO_2/SiO_2/Si$. In general, ΔH is explained in terms of a combination of grain sizes and misorientations of grains.[9,20] However, grains were clearly discernible only for VO_2 films grown on $TiO_2/SiO_2/Si$ at 200 °C and grown on TiO_2/PI at 250 °C in our samples, and thus, we need other explanations for the growth temperature dependence of ΔH. It seems that ΔH increased with increasing structural defect densities. Considering XRD (Fig. 2), TEM (Fig. 3), and Raman data (Fig. 4), amorphous VO_2 films grown on TiO_2/PI should have more structural defect densities than those grown on $TiO_2/SiO_2/Si$, and this may be responsible for the larger ΔH. The hysteresis width may be affected by the size and orientations of ordered regions embedded in an otherwise amorphous phase. Vernardou *et al.* grew amorphous and granular VO_2 films on glass substrates using atmospheric pressure chemical vapor deposition and reported that hysteresis widths decreased with increasing VO_2 short-range ordering.[28] This phenomenon may explain our data. The degree of crystallographic misorientation of grains between adjacent grains has been reported to be related to the hysteresis widths. During MIT, metallic regions can be propagated with smaller energy loss when the grain boundary misorientation angles are small.[29] Apparently, VO_2 films in this study may have ordered regions (i.e., marginally granular structures), and misorientation of ordered regions may be responsible for the change in hysteresis widths. The hysteresis curves in Figs. 5(e) and 5(f) were not closed for growth temperatures of 200 and 175 °C due to the heating effect, possibly because the thermal conductivity of PI is very low at 0.46 W/(m K).

VO_2 films on TiO_2-buffered PI substrates can be used for flexible smart windows, which automatically control the reflectivity when the temperature increases to above T_c. Figure 8 shows the reflectivity of VO_2 films grown on (a) $TiO_2/SiO_2/Si$ at 250 °C and on TiO_2/PI substrates at (b) 250 °C and (c) 175 °C. We measured the reflectivity of VO_2 films by using ellipsometry as the temperature was increased from RT to 100 °C. At 100 °C, the reflectivity increased in the infrared region due to MIT compared to that at RT.

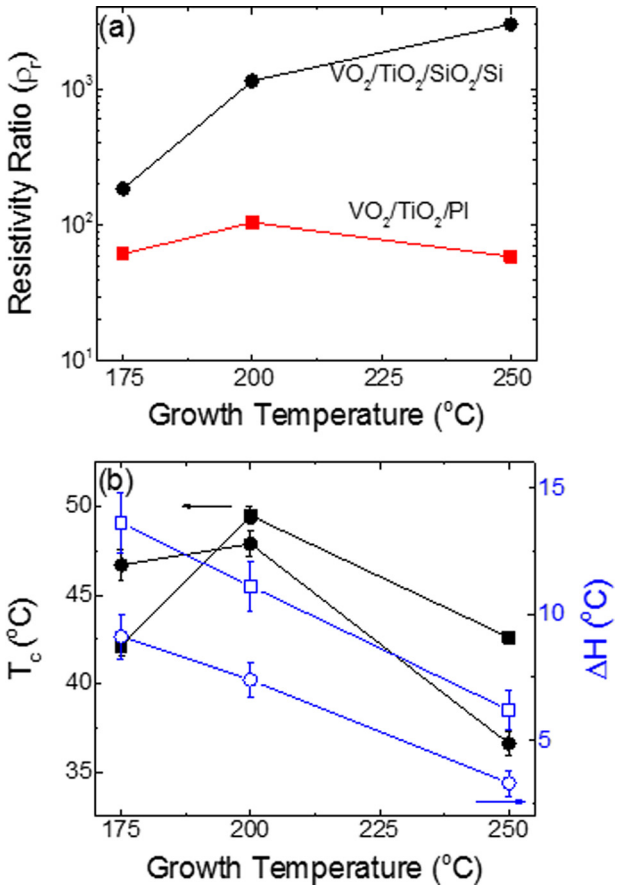

FIG. 7. (Color online) Plot of (a) the ratio (ρ_r) of resistivity throughout the MIT and (b) the transition temperature (T_c) and the hysteresis width (ΔH) of the VO_2 films grown on TiO_2/PI (circles) and $TiO_2/SiO_2/Si$ (rectangles) substrates.

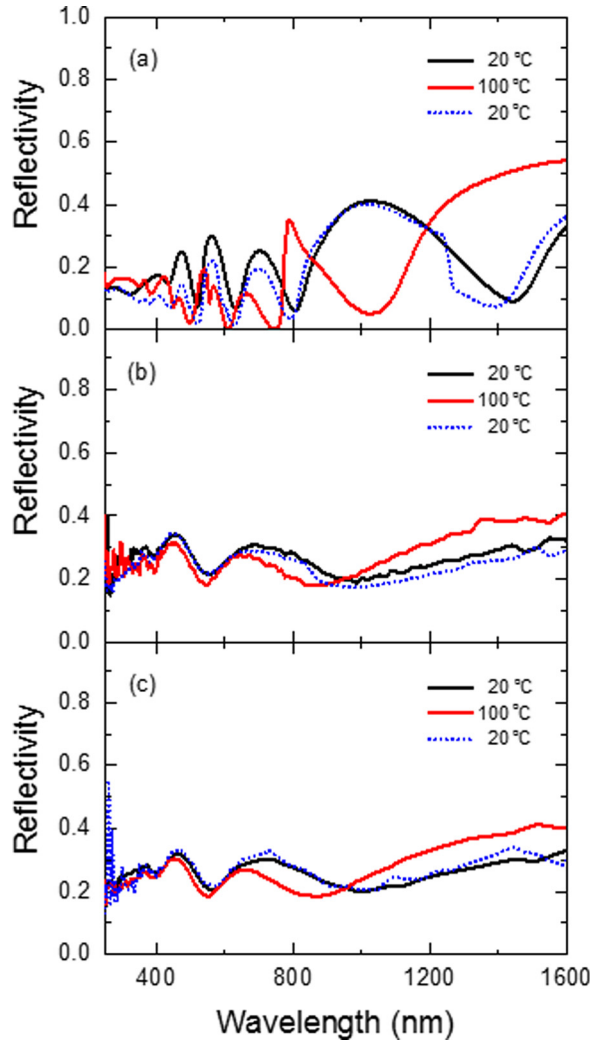

FIG. 8. (Color online) Reflectivity spectra of VO_2 films grown on (a) $TiO_2/SiO_2/Si$ (250 °C) and on TiO_2/PI substrates at (b) 250 °C and (c) 175 °C, which were measured at 20 °C [black (thick) lines] and 100 °C [red (dim) lines] under vacuum and at 20 °C in air (blue dotted lines).

The $VO_2/TiO_2/SiO_2/Si$ structure grown at 250 °C showed oscillating backside reflection effects, and the reflectivity at 1600 nm decreased from 54.0% to 32.9% throughout the MIT. The reflectivities of VO_2/TiO_2/PI films decreased from 40.7% to 32.5% (grown at 250 °C) and from 40.1 to 32.8% (grown at 175 °C) with the MIT. These changes in the reflectivity of the VO_2/TiO_2/PI films are comparable to those of highly crystalline VO_2 films grown on glass substrates reported in the literature,[30] even though the VO_2 films grown on TiO_2/PI in this work were amorphous. Our study shows that amorphous VO_2 films grown on TiO_2/PI substrates as low as at 175 °C are able to be used for thermochromic window applications.

In Fig. 5, the amorphous VO_2 films grown on TiO_2/PI showed a smaller portion of V^{4+} state XPS peaks compared to crystalline VO_2 films grown on $TiO_2/SiO_2/Si$. The areal ratio of the V^{4+} peak versus the sum of the V^{3+}, V^{4+}, and V^{5+} peaks was 62.3% (73.5%) for amorphous (crystalline) VO_2 films. As we mentioned in the Introduction, Youn *et al.* reported that the multivalence of V atoms affects the R-T hysteresis; This behavior occurs because increasing the phase of the V^{3+} and V^{5+} valence states over the phase of V^{4+} states decreases the contrast of the resistance as we change the stoichiometry of VO_{2+x}.[16] In our VO_2 films, amorphous films showed less R-T contrast than crystalline films during MIT due to the increasing structural disorder. This result is consistent with the finding that the proportion of V^{4+} states in the XPS spectra increased from the amorphous to crystalline phases. In VO_2 films, cation oxidation states strongly influence the electronic properties of VO_2 films.[16] In this work, structural disorder of amorphous VO_2 films due to broken long range order decreased the phase of V^{4+} states compared to that of crystalline VO_2 films and affected the R-T contrast.

In Figs. 5(a) and 5(c), we found the oxygen vacancy peak at 531.2 and 531.4 eV for the crystalline and amorphous VO_2 films, respectively, and $I(V_O)/I(O_{1s})$ increased from 22.2% to 32.8% with increasing disorder due to amorphization. However, we need a caution in the explanation. The so-called oxygen vacancy (V_O) peak (~531.3 eV) in Figs. 5(a) and 5(c) may have overlapped with the satellite peak (530.1 eV) of $V^{4+}{}_{2p3/2}$ and the satellite peak of $V^{5+}{}_{2p3/2}$ (530.9 eV),[22,31] and the discernment of the oxygen vacancy peak from the satellite peaks of $V_{2p3/2}$ was not possible in this work.

We note that the so-called oxygen vacancy (V_O) peak occurs from the shift of the binding energy of the O_{1s} core level due to the vacancy of neighboring oxygen atoms. The XPS V_O peak intensity increased with increasing oxygen deficiency in the oxide thin films, and the XPS V_O peak intensity was larger for amorphous metallic oxides than crystalline ones because the disorder of local bondings generated under-coordination of neighboring oxygen atoms for cation atoms. That is, the binding energy of the O_{1s} level shifted when the metallic cations are under-coordinated with neighboring oxygen atoms.[32,33] The binding energy shift of the V_O peak should depend on the nature of cations and local bonding structures in metallic oxides. For example, the binding energy shifts are +1.7 eV for ZnO,[34] +1.0 eV for ZnSnO,[35] +1.6 eV for In_2O_3,[36] and +1.3 eV for VO_2 films in this work. Because the vanadium atoms are multivalent and the corresponding local coordination varies depending on the valence state of the V atoms, the under-coordination of oxygen atoms around a vanadium atom is not so well defined. For example, at high oxygen vacancy concentrations, VO_2 films can locally form a stable phase of V_2O_3, where vanadium atoms are fully coordinated with neighboring oxygen atoms. Therefore, the characteristics of the V_O XPS peak in VO_2 films are not well understood. According to Zhang *et al.*, the intensity of the oxygen vacancy peak in VO_2 films was not proportional to the degree of oxygen deficiency in VO_2 films.[37] The nature of so-called oxygen vacancy peaks in the XPS spectra of metallic oxides needs more detailed investigation for both single- and multivalent metallic oxides.

Our work shows that the sizable MIT phenomenon can occur for amorphous VO_2 films grown on flexible TiO_2-buffered PI substrates at a low temperature of 175 °C. The resistivity ratio (ρ_r) was limited to about sixty, and the near-infrared rejection rate was comparable to that of crystalline VO_2 films reported in the literature.[30] This suggests that amorphous VO_2 films can be applied to smart window applications by controlling the reflectivity in the near-infrared spectral range. Amorphous VO_2 films are lacking in crystalline lattice periodicity. However, it seems that short range ordering persists in amorphous VO_2 films, which can manifest as quasi-MIT phenomena. MIT is associated with monoclinic to rutile transitions in crystalline VO_2 films. Quasi-MIT may occur in amorphous VO_2 films due to the transformation of local short range order between monoclinic-like and rutile-like atomic arrangements. Stephanovich *et al.* reported a short range order of approximately 1 nm for amorphous VO_2 films, which was estimated using x-ray diffraction spectra. They could generate the experimental XRD curves assuming a random assembly of 0.5 nm radius of spherical VO_2 nanocrystalline clusters.[38] Metallization in amorphous-to-amorphous transformation in Ge films was found using high pressure according to Di Cicco *et al.*[39] The details of local bond arrangements in amorphous VO_2 films can be studied using x-ray absorption fine structure spectroscopy, which is beyond the scope of this work.

Metal-insulator transition causes a significant change in the electrical and optical properties of crystalline VO_2 films near the transition temperature. The large contrast of resistivity change as large as 10^4 to 10^5 arises from metal-to-insulator transition in crystalline VO_2 films because free carrier concentrations and mobilities are significantly influenced by the metal-insulator transitions.[40] In amorphous VO_2 films, the resistivity change will be significantly lower than the crystalline VO_2 films because the lattice periodicities in VO_2 films are broken due to disorder of atomic bondings. For thermochromic applications such as smart windows, VO_2 films should be transparent in the UV-visible spectral range whether in metallic or insulating states, whereas switching of light rejection is required in the near-IR spectral range following metal-insulator transitions. For this purpose, the interband transition energies should be larger than 3 eV whether in metallic or insulating states, and the screened plasma frequency should fall on the near-IR, e.g., 1 eV, in the metallic state to block the near-IR light.[40] This work shows that amorphous VO_2 films can provide the desired thermochromic properties which are comparable to crystalline VO_2 films. It appears that the interband transition energies and the screened plasma frequency do not change much whether in crystalline or amorphous phases of VO_2 films because short range order of local atomic bonding is preserved in amorphous VO_2 films even though long range order is broken. Therefore, the reflectivity change in amorphous VO_2 films is still significant because the optical properties are less influenced by the breaking of long range order than the electrical properties of amorphous VO_2 films.

In general, VO_2 films grown on the rutile TiO_2 substrate showed low T_c values due to the misfit strain between VO_2 films and TiO_2 substrates or buffer layers.[8] This work, however, shows that VO_2 films grown on anatase TiO_2 buffer layers can still have low T_c values, $T_c = 47.6$ °C for VO_2/TiO_2/PI, possibly due to small grain sizes. A more detailed study is needed to verify the mechanism of low T_c values of VO_2 films grown on anatase TiO_2 buffer layers.

IV. CONCLUSION

We utilized the anatase TiO_2-layer-buffered SiO_2/Si and PI substrate to deposit VO_2 films at 175, 200, and 250 °C. VO_2 thin films grown on the TiO_2-buffered SiO_2/Si were crystallized at the growth temperatures of 200 and 250 °C and were amorphous at the growth temperature of 175 °C. The VO_2 films on TiO_2-buffered PI substrates were amorphous at growth temperatures of 175, 200, and 250 °C. We discussed the multivalence states of vanadium atoms and the oxygen vacancy peaks in the XPS spectra of crystalline and amorphous VO_2 films. Even for the VO_2 films grown on the TiO_2-buffered PI at 175 °C, the resistivity changed by almost 2 orders of magnitude with T_c (= 47.6 °C). The VO_2/TiO_2/PI films showed a change in reflectivity in the NIR with T_c, which was comparable to well-crystallized VO_2 films grown on glass substrates previously reported in the literature.[25] We showed that amorphous VO_2 thin films grown on flexible TiO_2/PI substrates at 175 °C can be used for thermochromic windows.

ACKNOWLEDGMENTS

H. Lee was supported by the National Research Foundation (NRF) in Korea, Grant No. 2016R1D1A1B03930725. S. Yoon was supported by NRF-2016R1D1A1B01009032. S. Y. Kim was supported by the Institute for Basic Science (IBS) in Korea, Grant No. IBS-R009-D1. H. Lee is grateful to T. W. Noh at the Seoul National University for the support on reflectivity measurements and to Ji Sang Park and Su-Huai Wei, formerly at NREL, for a preliminary calculation of the so-called XPS oxygen vacancy peak.

[1]M. Imada, A. Fujimori, and Y. Tokura, Rev. Mod. Phys. **70**, 1039 (1998).
[2]G. A. Niklasson, S. Y. Li, and C. G. Granqvist, J. Phys.: Conf. Ser. **559**, 012001 (2014).
[3]D. Zhang, M. Zhu, Y. Liu, K. Yang, G. Liang, Z. Zheng, X. Cai, and P. Fan, J. Alloy. Compd. **659**, 198 (2016).
[4]E. Gagaoudakis, G. Michail, E. Aperathitis, I. Kortidis, V. Binas, M. Panagopoulou, Y. S. Raptis, D. Tsoukalas, and G. Kiriakidis, Adv. Mater. Lett. **8**, 757 (2017).
[5]C.-I. Li *et al.*, Chem. Mater. **28**, 3914 (2016).
[6]M. O. Hakim, S. M. Babulanam, and C. G. Granqvist, Thin Solid Films **158**, L49 (1988).
[7]H. Kim *et al.*, ACS Nano **7**, 5769 (2013).
[8]Y. Muraoka and Z. Hiroi, Appl. Phys. Lett. **80**, 583 (2002).
[9]H. Koo, L. Xu, K.-E. Ko, S. Ahn, S.-H. Chang, and C. Park, J. Mater. Eng. Perform. **22**, 3967 (2013); and references therein.
[10]K. Miyazaki, K. Shibuya, M. Suzuki, H. Wado, and A. Sawa, J. Appl. Phys. **118**, 055301 (2015).
[11]A. W. Czanderna, C. N. R. Rao, and J. M. Honing, Trans. Faraday Soc. **54**, 1069 (1958).
[12]J. A. Koza, Z. He, A. S. Miller, and J. A. Switzer, Chem. Mater. **23**, 4105 (2011).
[13]D.-H. Youn, J.-W. Lee, B.-G. Chae, H.-T. Kim, S.-L. Maeng, and K.-Y. Kang, J. Appl. Phys. **95**, 1407 (2004).
[14]Y. Zhao, C. Chen, X. Pan, Y. Zhu, M. Holtz, A. Bernussi, and Z. Fan, J. Appl. Phys. **114**, 113509 (2013).
[15]N. Bahlawane and D. Lenoble, Chem. Vap. Deposition **20**, 299 (2014).
[16]D.-H. Youn, H.-T. Kim, B.-G. Chae, Y.-J. Hwang, J.-W. Lee, S.-L. Maeng, and K.-Y. Kang, J. Vac. Sci. Technol., A **22**, 719 (2004).
[17]C. Yang, H. Fan, Y. Xi, J. Chen, and Z. Li, Appl. Surf. Sci. **254**, 2685 (2008).
[18]Joint Committee on Powder Diffraction Standards, International Centre for Diffraction Data, No. 82-0661.
[19]Joint Committee on Powder Diffraction Standards, International Centre for Diffraction Data, No. 89-4921.
[20]D. H. Jung, H. S. So, K. H. Ko, J. W. Park, H. Lee, T. T. T. Nguyen, and S. Yoon, J. Korean Phys. Soc. **69**, 1787 (2016); and references therein.
[21]J. Zhang, M. Li, Z. Feng, J. Chen, and C. Li, J. Phys. Chem. B **110**, 927 (2006); and references therein.
[22]G. Silversmit, D. Depla, H. Poelman, G. B. Marin, and R. De Gryse, J. Electron Spectrosc. Relat. Phenom. **135**, 167 (2004).
[23]D. Brassard, S. Fourmaux, M. Jean-Jacques, J. C. Kieffer, and M. A. El Khakani, Appl. Phys. Lett. **87**, 051910 (2005).
[24]J. Cao *et al.*, Nano Lett. **10**, 2667 (2010).
[25]E. Radue, E. Crisman, L. Wang, S. Kittiwatanakul, J. Lu, S. A. Wolf, R. Wincheski, R. A. Lukaszew, and I. Novikova, J. Appl. Phys. **113**, 233104 (2013).
[26]C. H. Griffiths and H. K. Eastwood, J. Appl. Phys. **45**, 2201 (1974).
[27]S. Singh, T. A. Abtew, G. Horrocks, C. Kilcoyne, P. M. Marley, A. A. Stabile, S. Banerjee, P. Zhang, and G. Sambandamurthy, Phys. Rev. B **93**, 125132 (2016).
[28]D. Vernardou, D. Louloudakis, E. Spanakis, N. Katsarakis, and E. Koudoumas, Sol. Energy Mater. Sol. Cell **128**, 36 (2014).
[29]J. F. De Natale, P. J. Hood, and A. B. Harker, J. Appl. Phys. **66**, 5844 (1989).
[30]J. M. Tomczak and S. Biermann, Phys. Status Solidi B **246**, 1996 (2009); and references therein.
[31]R. Zimmerman, R. Claessen, F. Reinert, P. Steiner, and S. Hüffner, J. Phys.: Condens. Matter **10**, 5697 (1998).
[32]D. B. Buchholz, Q. Ma, D. Alducin, A. Ponce, M. Jose-Yacaman, R. Khanal, J. E. Medvedeva, and R. P. H. Chang, Chem. Mater. **26**, 5401 (2014).
[33]J.-W. Park, H. S. So, H.-M. Lee, H.-J. Kim, H.-K. Kim, and H. Lee, J. Appl. Phys. **117**, 155305 (2015).
[34]H. Liu, F. Zeng, Y. Lin, G. Wang, and F. Pan, Appl. Phys. Lett. **102**, 181908 (2013).
[35]V. Kumar Jain, P. Kumar, M. Kumar, P. Jain, D. Bhandari, and Y. K. Vijay, J. Alloys Compd. **509**, 3541 (2011).
[36]C. Janowitz *et al.*, New J. Phys. **13**, 085014 (2011).
[37]Z. Zhang *et al.*, Phys. Rev. Appl. **7**, 034008 (2017).
[38]G. Stefanovich, A. Velichko, A. Pergament, and P. Boriskov, "Amorphous vanadium dioxide: the resist for electron-beam lithography," Surf. Rev. Lett. (to be published).
[39]A. Di Cicco, A. Congeduti, F. Coppari, J. C. Chervin, F. Baudelet, and A. Polian, Phys. Rev. B **78**, 033309 (2008).
[40]L. Zhang *et al.*, Nat. Mater. **15**, 204 (2016).